Applications of a Prognostic Turbulence Kinetic Energy in a Bulk Boundary-Layer Model

by

David A. Randall
Piers Sellers
and
Donald A. Dazlich

Department of Atmospheric Science
Colorado State University
Fort Collins, Colorado

Colorado
State
University

Department of
Atmospheric Science

Paper No. 437

APPLICATIONS OF
A PROGNOSTIC TURBULENCE KINETIC ENERGY
IN A BULK BOUNDARY-LAYER MODEL

by

David A. Randall[1], Piers Sellers[2]

and Donald A. Dazlich[1]

[1]Department of Atmospheric Science
Colorado State University
Fort Collins, CO   80523

[2]Department of Meteorology
University of Maryland
College Park, MD   20742

January 1989

Atmospheric Science Paper No. 437

ABSTRACT

Bulk models of the planetary boundary layer (PBL) conventionally rely on diagnostic forms of the turbulence kinetic energy (TKE) equation to determine the entrainment rate. During episodes of rapid deepening or shallowing, the local time rate of change of the vertically integrated TKE becomes significant compared to the difference between gross production and dissipation. Entrainment theories that neglect this term therefore require revision. A method is presented to determine the entrainment rate in a bulk PBL model that includes a prognostic TKE. Relative to earlier closures, the new method is not only more realistic but also easier to implement. An analytical expression for the entrainment rate is obtained for a broad class of cloud-free boundary layers.

A Wangara simulation is presented to illustrate the behavior of the model. The Simple Biosphere model (SiB) is used to predict the temperatures of the soil and vegetation at the Wangara site. The prognostic TKE leads to a slight improvement in the simulation.

The role of shallowing in a large-scale model is discussed. Tests of the prognostic TKE in the CSU general circulation model are briefly described.

1. Introduction

Neglecting horizontal advection and gravity-wave losses, the vertically integrated conservation law for the turbulence kinetic energy (TKE) of the planetary boundary layer (PBL) can be written as

$$g^{-1} \, \delta p_M \frac{\partial e_M}{\partial t} + E e_M = P - N - D.$$

(1.1)

Here g is the acceleration of gravity; δp_M is the pressure thickness of the PBL; E is the entrainment mass flux; e_M is the vertically averaged TKE; P is gross production of TKE by convection and shear; N is consumption by downward buoyancy fluxes; and D is dissipation. Transport terms arising from pressure-velocity correlations and triple velocity correlations have dropped out of this vertically integrated equation, because we have assumed that the transports vanish at the earth's surface and above the PBL top. The definitions of P and N, and methods to determine them, are discussed later.

In most situations, both terms on the left-hand side of (1.1) are quite negligible. During brief but important episodes of rapidly changing PBL depth, however, the $E e_M$ term of (1.1), which is sometimes called the "storage" term, can become significant. This was pointed out by Zilitinkevitch (1975) and Kim (1976), who nevertheless assumed that the local time rate of change of e_M can be neglected in (1.1) even when the PBL depth is changing rapidly. A simple argument suggested by J. W. Deardorff (personal communication, 1979) shows that this assumption is not generally valid. Let R be the ratio of the two terms on the left-hand side of (1.1), i.e.

$$R \equiv \left(g^{-1} \, \delta p_M \frac{\partial e_M}{\partial t} \right) / \left(E e_M \right).$$

(1.2)

Our goal is to demonstrate that it is quite possible for R to be of order 1. For convenience, define $\sigma^2 = e_M$, so that

$$\frac{\partial e_M}{\partial t} = \frac{\partial \sigma^2}{\partial t} = \frac{2}{3} \frac{1}{\sigma} \frac{\partial \sigma^3}{\partial t}.$$

(1.3)

Using (1.3) in (1.2), we obtain

$$R \equiv \left(\frac{2}{3} g^{-1} \, \delta p_M \frac{\partial \sigma^3}{\partial t} \right) / \left(\sigma^3 E \right).$$

(1.4)

Consider the clear convective PBL, and suppose that $\sigma \sim w_*$, where w_* is the convective velocity scale of Deardorff (1970), which can be written as

$$w_*^3 = \kappa \frac{(F_{sv})_s}{(\rho p)_s} \delta p_M.$$

(1.5)

2

Here κ is Poisson's constant, F_{sv} is the virtual dry static energy flux, ρ is density, p is pressure, and subscript S denotes a surface value. Consider a case in which

$$\frac{\partial}{\partial t}\left[\kappa \frac{(F_{sv})_S}{(\rho\, p)_S}\right] = 0.$$

(1.6)

The time change of the PBL depth satisfies

$$\frac{\partial}{\partial t}\, \delta p_M = g E \,,$$

(1.7)

when large-scale divergence and cumulus convection are negligible. Use of (1.5-7) in (1.4) gives R = 2/3. This strongly suggests that on occasions when the PBL depth is changing rapidly, the local time rate of change of e_M can be significant in (1.1). Confirmation of this by numerical examples will be given later.

Keeping the local time rate of change essentially means developing a bulk PBL model that uses (1.1) to determine the TKE prognostically, i.e., by time-stepping from an initial value. The remainder of this paper describes such a model, presents numerical results to illustrate its performance, and provides further evidence that a prognostic TKE can be useful in modeling the bulk structure of the PBL.

2. Closure

Following the approach of Randall (1979; also see Suarez *et al.*, 1983), the vertically integrated dissipation rate and the vertically averaged TKE are assumed to be related by

$$D = \rho_M \left(e_M / a_1\right)^{3/2},$$

(2.1)

where ρ_M is the vertically averaged PBL density, and $a_1 \cong 0.163$ is a dimensionless constant.

In conventional entrainment theories, it is assumed that dissipation is proportional to gross production; i.e.,

$$D = a_2 P,$$

(2.2a)

where $a_2 \cong 0.96$ is a second dimensionless constant (Randall, 1984); and it is also assumed that the local time-derivative term of (1.1) is negligible (Zilitinkevich, 1975; Kim, 1976). With these assumptions, (2.2a) can be combined with (1.1) and (2.1) to obtain

$$e_M E + N = \tilde{D} \,,$$

(2.2b)

where

$$\tilde{D} \equiv \rho_M \left(\frac{1 - a_2}{a_2} \right) \left(\frac{e_M}{a_1} \right)^{3/2} .$$

(2.3)

This result states that the sum of "storage" and consumption is a constant fraction of dissipation. When the local time-rate-of-change term of (1.1) is neglected, (2.2a) and (2.2b) are equivalent.

If we use (2.1) and (2.2a) in (1.1), we get

$$g^{-1} \delta p_M \frac{\partial e_M}{\partial t} + E e_M = - N + \rho_M \left(e_M / a_1 \right)^{3/2} \left(\frac{1 - a_2}{a_2} \right) .$$

(2.4a)

Inspection suggests and experiment confirms that the last term on the right-hand side of (2.4a) leads to exponentially growing TKE; our assumptions have thus led us to an unrealistic result. This means that, in a sense, (2.1) and (2.2a) are not consistent with (1.1).

As an alternative, we can use (2.1) and (2.2b) in (1.1) to obtain

$$g^{-1} \delta p_M \frac{\partial e_M}{\partial t} = P - \frac{\rho_M}{a_2} \left(\frac{e_M}{a_1} \right)^{3/2} .$$

(2.4b)

According to (2.4b), if P varies slowly with time, e_M will approach a quasiequilibrium value such that $(e_M)^{3/2}$ is proportional to P. In fact, the same quasiequilibrium relationship between P and e_M can be obtained by eliminating D between (2.1) and (2.2a). From (2.4b), it is clear that the time scale for the equilibration of e_M with P is

$$\tau_{adj} = a_2 \, \delta z_M \sqrt{\frac{a_1}{e_M}} ,$$

(2.5)

where δz_M is the geometrical depth of the PBL. Using the values of a_1 and a_2 given above, with $\delta z_M = 500$ m and $e_M = 0.5$ m^2 s^{-2}, we find that τ_{adj} is about 5 minutes. Of course, τ_{adj} increases with increasing PBL depth, and decreases with increasing turbulence intensity. Clearly, (2.4b) predicts a realistic coevolution of e_M and P that is consistent with conventional entrainment parameterizations so long as $\partial e_M / \partial t$ is negligible in (1.1). In the present model, (1.1) [or (2.4b)] is used to predict the TKE, and (2.2b) is used as a closure condition to determine the entrainment mass flux.

Since e_M is nonnegative, (2.2b) implies that the sign of E is the same as the sign of $\tilde{D}$ - N. Negative values of E imply a "shallowing" of the PBL that, according to (2.2b), occurs when the consumption rate exceeds $\tilde{D}$. The physical mechanism of shallowing and the role of shallowing in the present model are discussed in Section 5. For now, we note that $\tilde{D}$ depends only on e_M and is parametrically independent of E; and we assume that N is a nondecreasing function of E for E > 0, and is independent of E for E < 0. A justification of these assumptions concerning N(E) will be given later. The assumptions imply that the smallest possible value of N occurs for E = 0. Then, as indicated in Figure I, there is always a unique solution for E, whose sign agrees with that of $\tilde{D}$ - N (E=0).

4
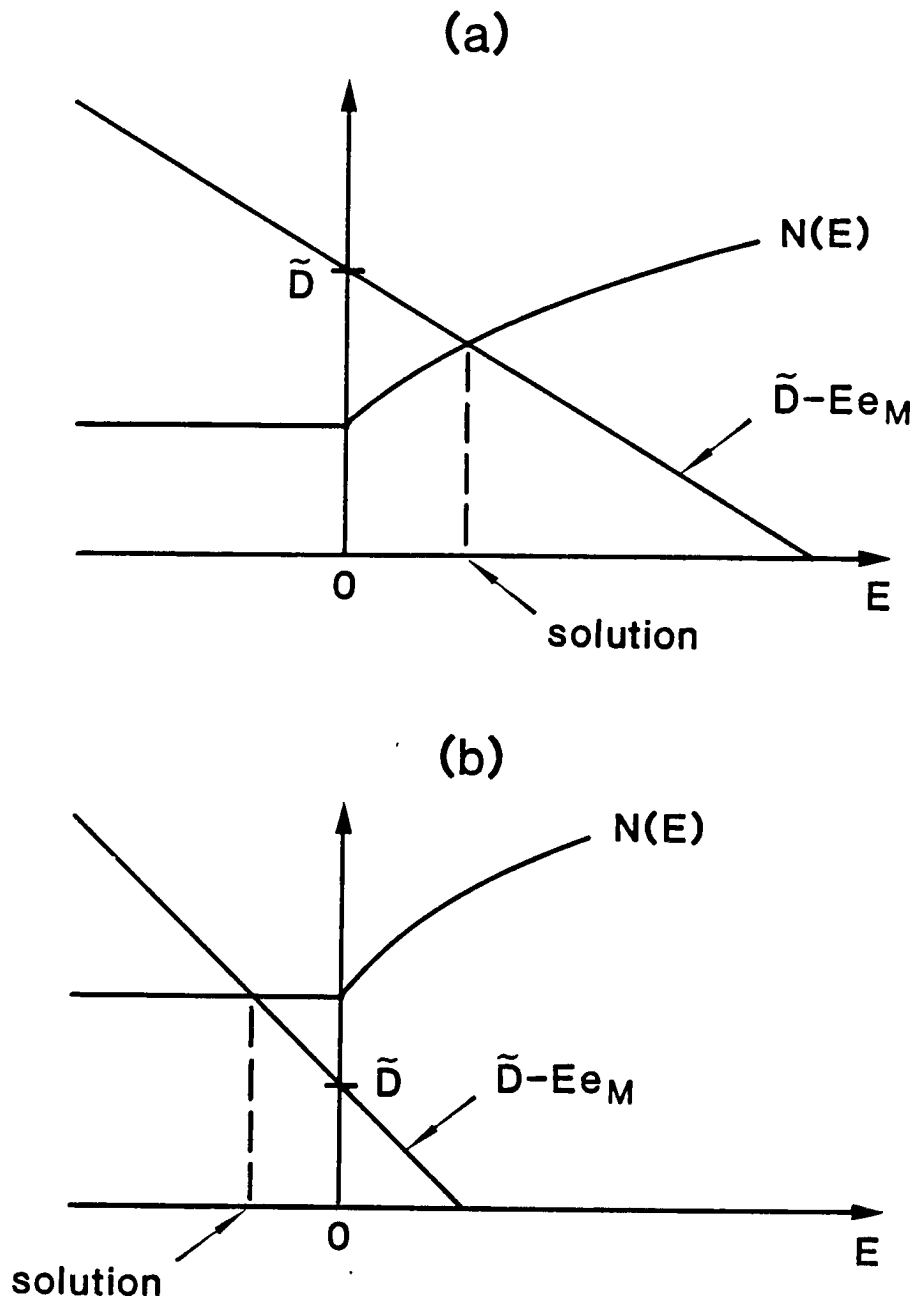
Figure 1: Diagram illustrating the existence of a unique solution for the entrainment rate, E: a) E > 0; b) E < 0 .

3. Method of solution

a) *Analytical solution for cloud-free mixed layers.* The preceding discussion has not made use of any particular definitions of P and N; it has only been assumed that N is a nondecreasing function of E. We now adopt "Eulerian partitioning," as discussed by Randall (1984), in order to study some particular solutions of the model.

For cloud-free convective well mixed layers, it is well known (e. g., Ball, 1960) that $F_{sv}(p)$ is linear. The consumption rate can be written as

$$N = \frac{1}{2} \kappa \frac{\delta p_M}{p_B} \left[\frac{\left(E \Delta s_v \right)^2}{\left(F_{sv} \right)_s + E \Delta s_v} \right],$$

(3.1)

where Δs_v is the "jump" in virtual dry static energy at the mixed-layer top, which is assumed to be nonnegative[1]. Substituting (3.1) into (2.2b), and rearranging, we find that E satisfies a quadratic equation with known coefficients:

$$E^2 \left[e_M \Delta s_v + \frac{1}{2} \kappa \frac{\delta p_M}{p_B} (\Delta s_v)^2 \right] + E \left[e_M (F_{sv})_s - \Delta s_v \right] - \tilde{D} (F_{sv})_s = 0.$$

(3.2)

For $\Delta s_v = 0$, (3.2) reduces to

$$E = \tilde{D} / e_M = \rho_M \left(\frac{1 - a_2}{a_2} \right) \sqrt{\frac{e_M}{a_1^3}}.$$

(3.3)

Generally, (3.3) holds whenever N = 0 [see (3.1)]. In solving (3.2), the plus sign must be chosen for the discriminant. For $(F_{sv})_s = 0$, (3.2) reduces to

$$E = \tilde{D} / \left(e_M + \frac{1}{2} \kappa \frac{\delta p_M}{p_B} \Delta s_v \right),$$

(3.4)

which is positive. This shows that a necessary condition for E < 0 is $(F_{sv})_s < 0$.

---

[1] When applying the results of this Section, negative values of Δs_v should be replaced by zero, and it is assumed that $\Delta s_v = 0$ for E < 0. Here a comment is needed concerning the assumption that the "jumps" vanish for E < 0. In the case of s_v, for example this implies that $(s_v)_{B+} = s_{vM}$ for E < 0. However, we *cannot* make the analogous assumption that $e_{B+} = e_M$ for E < 0, since e_{B+} must always be equal to zero. Instead, we must assume that e decreases continuously to zero at the PBL top, at least for E < 0.

Now suppose that $F_{sv}(p) < 0$ throughout the PBL. We continue to assume that $F_{sv}(p)$ is linear. Then the consumption rate is given by

$$N = \frac{1}{2}\kappa\frac{\delta p_M}{p_B}\left[\frac{E\Delta s_v}{p_B} - \frac{(F_{sv})_s}{p_s}\right],$$

(3.5)

Use of (3.5) in (2.2b) gives an expression for the entrainment rate:

$$E = \frac{\tilde{D} + \frac{1}{2}\kappa\frac{\delta p_M}{p_s}(F_{sv})_s}{\theta_M + \frac{1}{2}\kappa\frac{\delta p_M}{p_B}\Delta s_v}.$$

(3.6)

For $(F_{sv})_s = 0$, (3.6) agrees with (3.4). The denominator of (3.6) is positive, so the sign of E is determined by the sign of the numerator; $E < 0$ occurs for

$$(F_{sv})_s < \frac{-2\tilde{D}\,p_s}{\kappa\delta p_M} < 0.$$

(3.7)

According to (3.7), $E < 0$ is associated with or forced by a sufficiently negative surface buoyancy flux. The required negative flux increases as the TKE increases, since $\tilde{D} \sim (e_M)^{3/2}$. Interestingly, the required negative flux decreases as δp_M increases. This means that it is "easier" to cause a boundary layer to undergo shallowing when it is deep than when it is already shallow.

b) *Cloud-topped mixed layers.* The cloud-topped mixed layer has a complicated buoyancy flux profile, featuring abrupt changes at cloud base and just below cloud top. Negative values can occur in various places, depending on the entrainment rate and other factors. When presented with buoyancy flux profiles of such complexity, Eulerian partitioning does not provide an analytical solution for E. A unique solution is nevertheless guaranteed, as long as N is a nondecreasing function of E. This is the case when the inversion is sufficiently strong. The solution can be obtained by a straightforward iterative method. Further details are given by Randall (1984) and references therein.

4. Tests with a one-dimensional model

To illustrate the behavior of the prognostic model [which keeps the time derivative in (1.1)] and to show how it differs from the more conventional diagnostic model [which neglects the time derivative in (1.1)], we consider the "standard" Wangara Day 33 case that has been studied by so many authors. The surface-flux parameterization used is based on that of Deardorff (1972). The time-differencing methods are described in Appendix A. The time-step used is 100 s. Lower limits of 0.2 $m^2 s^{-2}$ and 1 mb are imposed on the TKE and PBL depth, respectively, unless otherwise specified.

The surface temperature and evapotranspiration are predicted using the Simple Biosphere (SiB) model of Sellers *et al.* (1986), modified slightly to use the "force-restore" method (Bhumralkar, 1975). The data of Clarke *et al.* (1971) are used to prescribe, as functions of time, the sounding of the free atmosphere, the geostrophic wind, and the net surface radiation. The starting time for the

simulations is 0900 local time (LT). The initial conditions are given in Table 1. The SiB input parameters for the Wangara site are given in Tables 2 and 3.

Fig. 2 shows the simulated time-evolution of the PBL depth; TKE; screen temperature at 1.3 m above the surface; inversion strength; soil heat flux; and the adjustment time scale defined by (2.5). Also shown for comparison are the corresponding results with the diagnostic model described by Randall (1979), as well as available observations. The two models give generally similar results, as would be expected. The prognostic model predicts a more rapid morning deepening, a greater afternoon depth, slightly later shallowing, and a greater nocturnal depth. The TKE reaches larger values during the day in the prognostic model; the imposed minimum also ensures larger values at night. The nocturnal screen temperatures are considerably warmer in the prognostic model. The afternoon inversion strength is greater, reflecting the deeper penetrations of the PBL into the stratified free atmosphere, but the nocturnal inversion is weaker, since the PBL is warmer. The nocturnal soil heat flux is more strongly negative in the prognostic model. Both models produce afternoon adjustment time scales on the order of 1/3 hour, decreasing rapidly at sunset to values on the order of a minute. The predicted afternoon adjustment times are on the order of the lifetime of a large thermal.

Fig. 3 shows the ratio of w_e (the entrainment velocity) to w· (the convective velocity scale), as simulated by the prognostic model. During rapid deepening, when the inversion has been wiped out by surface warming and the PBL is entraining into an isentropic layer, this ratio approaches 0.2, as in the large-eddy simulation of Deardorff (1974). Fig. 4 shows the relative magnitudes of the local time-rate of change of θ_M and the conventional storage term. During rapid deepening and shallowing, both expressions are of order 1, confirming the analysis presented earlier.

After sunset, the TKE remains constant at its prescribed minimum value of 0.2 $m^2 s^{-2}$, while the PBL depth remains nearly constant at about 90 m. This is the depth for which N and $\tilde{D}$ balance in (2.2b), where $\tilde{D}$ is determined by the prescribed minimum TKE. The effect of using a larger minimum TKE is like that of turning on fans in an orchard at night: stirring is produced through a deeper layer, the surface is warmed, and sensible heat is transported downward.

Considering its extreme simplicity, the prognostic bulk model reproduces the observed evolution of the boundary layer remarkably well.

5. Comments on shallowing

The concept of shallowing is closely identified with the "evening transition" that characteristically occurs as part of the diurnal cycle of the PBL over land, although rapid decreases in PBL depth may also occur (at any time of day) in conjunction with weather events such as warm-frontal passages. Observations of the evening transition are discussed by Mahrt (1981). Shallowing also occurs in the upper ocean; in fact, shallowing was first modeled as a continuous rapid decrease of the mixed layer. The effects are similar: a deep turbulent layer is replaced, over a short period of time, by a shallower turbulent layer. The deep well mixed layer is typically observed to persist long after the turbulence that produced it has decayed.

Bulk models of the PBL are capable of simulating some of the observed features of both deep convective mixed layers and shallow shear-driven nocturnal PBLs. It seems unlikely, however, that they can also simulate the actual mechanisms of the shallowing transitions between these PBL types. A premise of all bulk models is that the PBL is well defined and, in particular, that it has a well-defined top. This may not be true during shallowing. Some observations indicate that, as the evening transition begins, turbulence is extinguished most rapidly near the surface, leaving a detached and decaying turbulent layer above. At this point, does a turbulent PBL really exist, and if so where is its top?

Table 1: Initial conditions for the Wangara simulation.

$$\delta p_M = 18 \text{ mb}$$
$$\theta_M = 277.6 \text{ K}$$
$$r_M = 3.7 \text{ g kg}^{-1}$$
$$u_M = 7 \text{ m s}^{-1}$$
$$v_M = 0.3 \text{ m s}^{-1}$$
$$e_M = 0.2 \text{ m2 s}^{-2}$$
$$T_g = 286 \text{ K}$$
$$T_c = 286 \text{ K}$$
$$T_d = 276 \text{ K}$$
$$W_1 = 0.1$$
$$W_2 = 0.1$$
$$W_3 = 0.1$$
$$M_c = 0$$
$$M_g = 0$$

Table 2: SiB input parameters for the Wangara site, obtained from the following sources: variables marked with * were obtained from the data set described by Willmott and Klink (1986), as modified by Dorman and Sellers (personal communication); variables marked with + were estimated from the photographs and descriptions of the site as published by Clarke *et al.* (1971).

Parameters	Units	Numerical Value	Remarks
PLANT MORPHOLOGY			
Height of canopy top	m	0.4	+
Ground roughness length	m	0.005	+
Leaf area index		1.0	*, +
Leaf angle distribution factor		0.1	*
Leaf drag coefficient		0.106	*, +
Leaf shelter factor		4.0	*, +
Upper storey cover fraction		0.3	+
Root density	m m^{-3}	3600.	*
Root depth	m	0.5	*
Root cross section	m	2 4x10^7	*
Root resistance	s m^{-1}	4x10^{12}	*
Stem resistances		2.5x10^8	*
Leaf reflectance (VIS, NIR)		0.28, 0.48	*
Leaf transmission (VIS, NIR)		0.018, 0.068	*
Live leaf fraction		0.20	*
SOIL			
Soil moisture potential at saturation	m	-0.167	*
Soil moisture potential parameter		4.80	*
Soil sat. condition.	m s^{-1}	7.65x10^{-5}	*
Porosity		0.435	*
Soil moisture store depths	m	0.02, 0.48, 0.50	
Soil reflectance (visible, near infrared)		0.25, 0.30	+

Table 3: Derived aerodynamic parameters for the Wangara site, calculated using a modification of the methodology described in the Appendix of Sellers *et al.* (1986).

Roughness length	z_0	0.022 m
Zero plane displacement	$d_0.$	177 m
Canopy transfer coefficient	C_1	81.97 s m^{-1}
Soil to canopy transfer coefficient	C_2	80.50
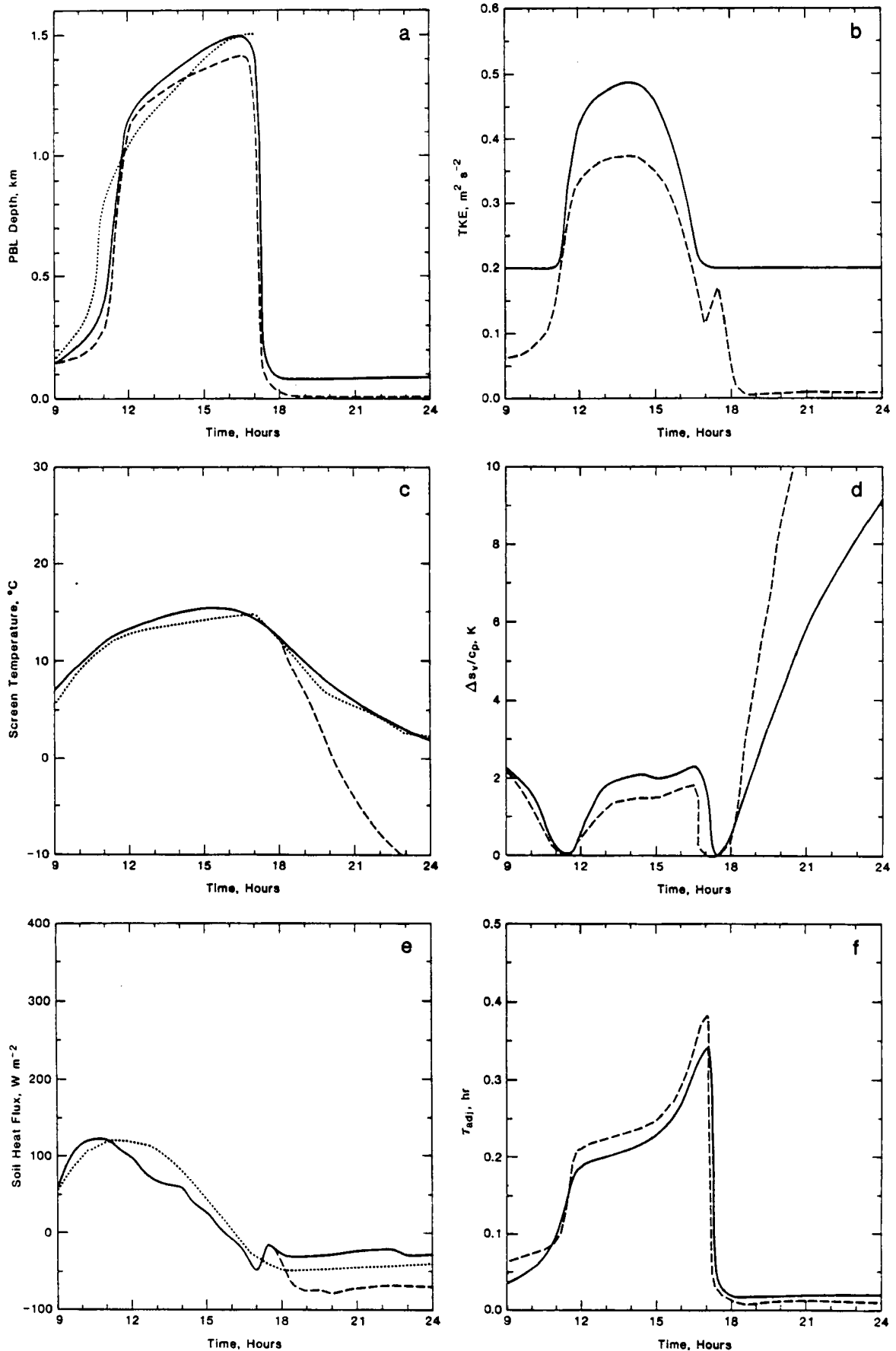
Figure 2: Results for Wangara Day 33: a) PBL depth; b) TKE; c) screen temperature; d) inversion strength; e) soil heat flux; f) adjustment time scale for the TKE. Solid and dashed lines show simulations with the prognostic and diagnostic models, respectively; dotted lines show the observations of Clarke *et al.* (1971), where available, except that for the PBL depth the dotted line shows results from the large-eddy simulation of
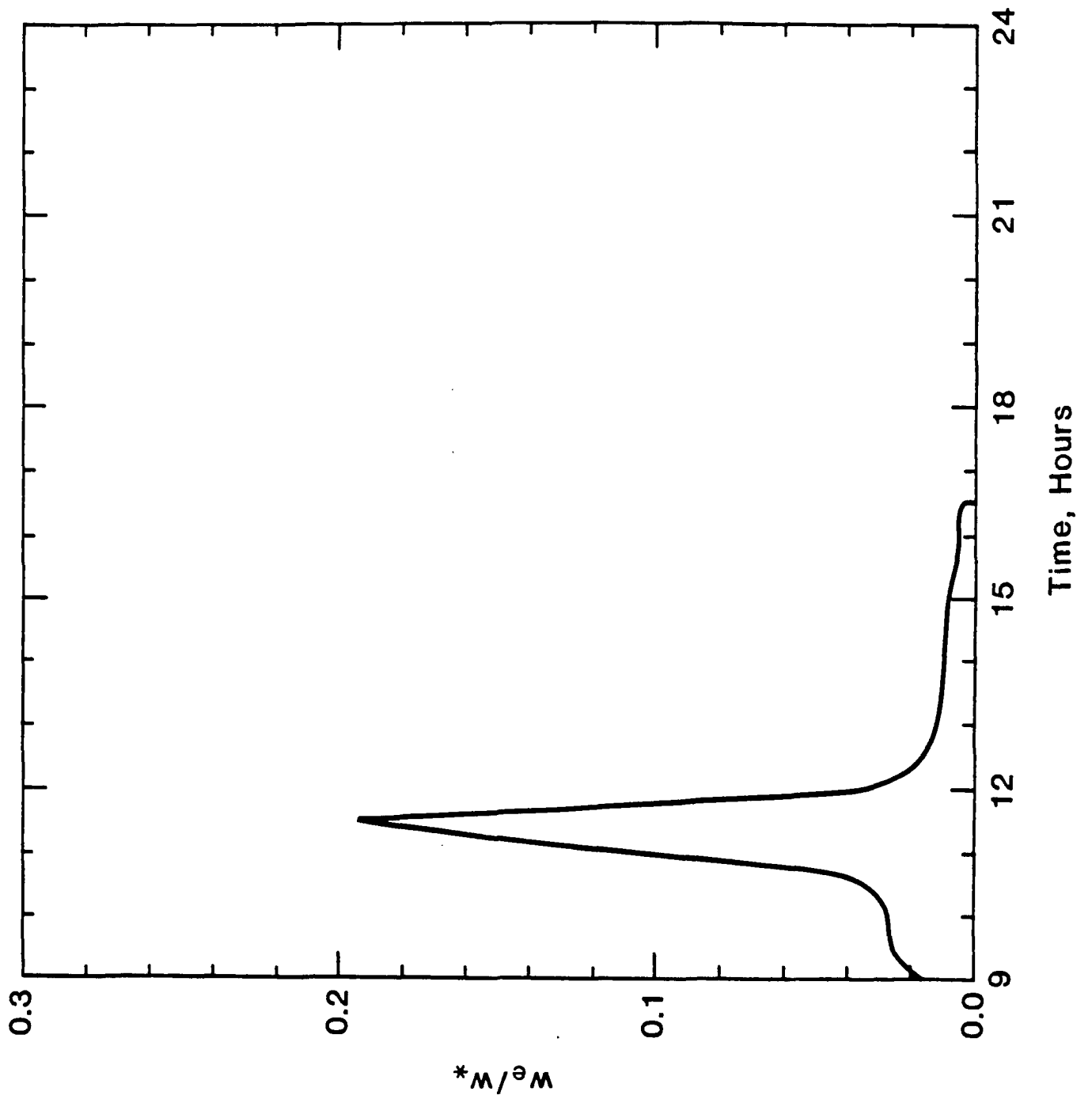
Figure 3:   Prognostic model simulation of w_e/w_*, for Wangara Day 3.
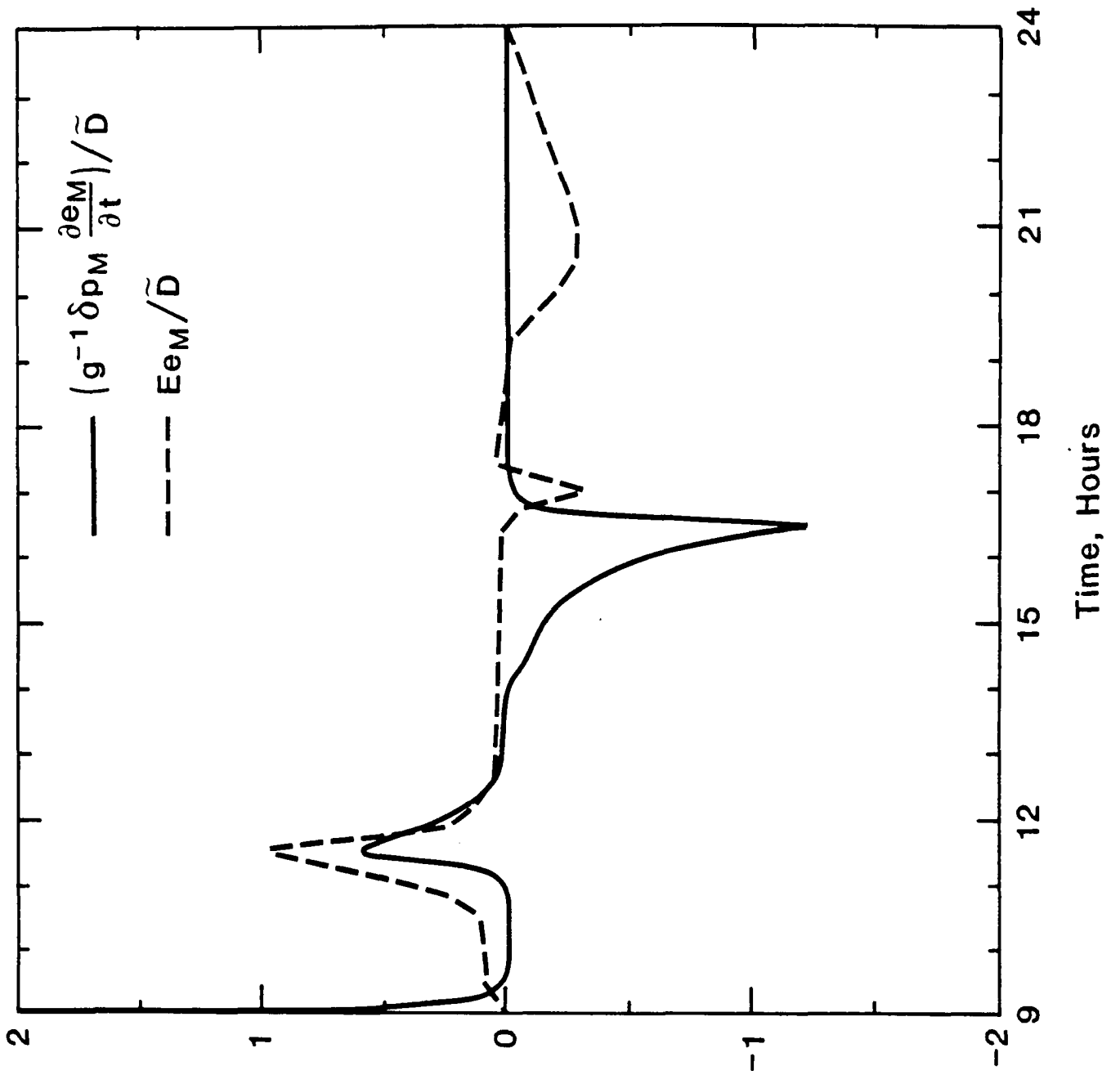
Figure 4:   As in Figure 3, but for two terms of the TKE conservation equation.

After the shallowing event has ended, a shallow, shear-driven turbulent layer grows upward from the surface, and the residual upper-level turbulence is quenched.

For large-scale modeling, the actual mechanisms of a shallowing event are not important; the event is brief, and it occurs at a time when the turbulent fluxes are weak anyway. The most important consequence of shallowing, from a large-scale point of view, is that air which has been inside the PBL and subject to strong turbulent coupling with the boundary is released by shallowing into the nonturbulent free atmosphere. The daily cycle of deepening and shallowing "captures" free atmospheric air, charges it with surface-like properties, and then releases it. A large-scale model must simulate this process. In addition, the shallowing must occur at the right time and place, and must provide suitable "initial conditions" for the nocturnal PBL. The Wangara simulation presented in Section 4 provides evidence that the bulk model can meet these requirements.

6. Tests with the CSU general circulation model

As described by Suarez et al. (1983), the UCLA GCM contains a PBL parameterization with a prognostic PBL depth whose time rate of change is determined, in part, through an entrainment parameterization. A parameterization of PBL stratus clouds and an explicit coupling of the PBL and cumulus parameterizations are important features of the model. Baseline results and sensitivity tests were presented by Randall et al. (1985). A modified version of the model, now called the CSU GCM, is being used in climate studies at Colorado State University. The most important difference between the UCLA GCM and the CSU GCM is that the latter uses the terrestrial and solar radiation parameterizations described by Harshvardhan et al. (1987).

A prognostic TKE and the entrainment parameterization described in Section 2 have been tested in the GCM. The simple interactive biosphere model (SiB) used in the offline tests discussed in Section 5 was not used in the GCM run; tests of SiB in the GCM are currently under way and will be reported elsewhere. The initial conditions used were for 1 June (taken from an earlier long run with a different version of the model). Generally, the GCM's performance is similar with and without the prognostic TKE. The PBL variables are slightly smoother, and the entrainment calculation executes faster. A few results are presented here to illustrate the model's behavior.

The PBL deepens, on the average, over both land and ocean; the globally averaged PBL depth increases by about 70 meters. Recall that we also obtained a greater depth in the Wangara simulation. The mean potential temperature of the PBL rises, while the mean mixing ratio decreases and the mean wind speed increases. Each of these changes is small; each is consistent with slightly more vigorous entrainment of air from the warm, dry, and windy free atmosphere.

The surface sensible heat flux increases by 10 W m^{-2} over land, but it decreases by 4 W m^{-2} over the oceans; the global mean hardly changes. The surface latent heat flux increases by 4 W m^{-2} globally. The net surface energy flux, due to both turbulence and radiation, increases slightly, mainly over land. The surface energy budget has, overall, been noticeably perturbed by the introduction of the prognostic TKE. Unfortunately, the available observations are not reliable enough to show whether this perturbation amounts to an improvement in the model results.

In concert with the increased surface evaporation mentioned above, the precipitable water content of the global atmosphere increases by 1.5 mm, and the precipitation rate also increases, mainly over the tropical oceans.

These results should be regarded with caution, because they are based on a single monthly mean. Nevertheless, they illustrate two things. First, the prognostic TKE is behaving itself in the GCM. Second, the energy budget and hydrologic cycle of the global model are quite sensitive to the details of the boundary layer parameterization, which therefore should be formulated very carefully.

7. Summary and conclusions

We have presented a bulk boundary-layer model with a prognostic TKE; this can be described as a very poor man's second-order closure model. Development of the model was motivated by an analysis which suggests that the time-rate-of-change term of the vertically integrated TKE equation becomes significant during rapid deepening and shallowing. Our numerical results confirm this point, yet they also show that the overall behavior of the prognostic model differs only slightly from that of the diagnostic model. The prognostic TKE allows slightly more accurate simulation of rapid changes in the PBL depth; perhaps of more practical significance is the fact that it simplifies solution for the entrainment rate. In addition, it opens the door to further generalizations of the PBL parameterization, such as including the effects of small-scale fractional cloudiness.

ACKNOWLEDGEMENTS

APPENDIX A

Time-Differencing Scheme

An implicit time-differencing scheme is needed to avoid computational instability with long time steps. A suitable scheme can be based on (2.4b), which is repeated here for convenience:

$$g^{-1} \delta p_M \frac{\partial e_M}{\partial t} = P - \frac{\rho_M}{a_2} \left(\frac{e_M}{a_1} \right)^{3/2} .$$

$$(A.1)$$

The gross production rate, P, depends on the entrainment rate and, therefore, on the TKE, since the entrainment closure assumption involves the TKE. Experience has shown that this dependence of P on e_M must be taken into account in order to obtain a sufficiently stable time-differencing scheme.

Let P_0 be the value of P obtained if $E = 0$; clearly, P_0 is independent of e_M, because it is independent of the entrainment rate. We enforce

$$P < P_0 .$$

$$(A.2)$$

This is equivalent to limiting the shear-production of TKE that occurs as a result of entrainment. We can write (A.1) as

$$g^{-1} \delta p_M \frac{\partial e_M}{\partial t} = P_0 - \left[\frac{P_0 - P}{e_M} + \frac{\rho_M}{a_1 a_2} \sqrt{\frac{e_M}{a_1}} \right] e_M .$$

$$(A.3)$$

A simple backward-implicit-differencing scheme can be applied to (A.3), giving

$$e_M^{n+1} = \frac{e_M^n + \left(g \, \delta t / \delta p_M \right) P_0}{1 + \left(g \, \delta t / \delta p_M \right) \left(\frac{P_0 - P}{e_M^n} \right) + \frac{\rho_M}{a_1 a_2} \sqrt{\frac{e_M}{a_1}}} .$$

$$(A.4)$$

Here superscripts n and n+1 denote succeeding discrete times. This scheme has proven to be very stable, provided of course that (A.2) is satisfied.

REFERENCES

Arakawa, A., 1972: Design of the UCLA General Circulation Model. *Technical Report #7*, Department of Meteorology, University of California, Los Angeles, 116 pp.

Ball, F. K., 1960: Control of inversion height by surface heating. *Quart. J. Roy. Meteor. Soc.*, 86, 483-494.

Bhumralkar, C. M., 1975: Numerical experiments on the computation of ground surface temperature in an atmospheric general circulation model. *J. Appl. Meteor.*, 14, 1246-1258.

Camillo, P. J. and T. J. Schmugge, 1980: A computer program for the simulation of heat and moisture flow in soils, *NASA Tech. Mem. 82121*, NASA/GSFC, Greenbelt, MD 20771

Clarke, R. H., A. J. Dyer, R. R. Brook, D. G. Reid, and A. J. Troup, 1971:The Wangara experiment: Boundary Layer data. *Tech. Paper 19*, Div. Meteor. Phys., CSIRO, Australia.

Deardorff, J. W., 1970: Convective velocity and temperature scales for the unstable planetary boundary layer and for Rayleigh convection. *J. Atmos. Sci.*, 27, 1211-1213.

Deardorff, J. W., 1972: Parameterization of the planetary boundary layer for use in general circulation models. *Mon. Wea. Rev.*, 100, 93-106.

Deardorff, J.W., 1974: Three-dimensional numerical study of the height and mean structure of a heated planetary boundary layer. *Bound. Layer Meteor.*,7, 81-106.

Deardorff, J. W., 1977: Efficient prediction of ground surface temperature and moisture, with inclusion of a layer of vegetation. *J. Geophys. Res.*, 83, 1889-1903.

de Vries, D. A., 1975: *Heat transfer in soils*. Scripta Book Company, Washington, D. C., 594 pp.

Dickinson, R. E., 1983: Land surface processes and climate-surface albedos and energy balance. *Adv. in Geophys.*, 25, 305-353.

Garratt, J. R., 1978: Flux profile relations above tall vegetation, *Quart. J. Roy. Meteor. Soc.*, 104, 199-211.

Goudriaan, J., 1977: *Crop micrometeorology: A simulation study.* , Wageningen Center for Agricultural Publishing and Documentation. Wageningen, The Netherlands, 249.

Harshvardhan, R. Davies, D. A. Randall, and T. G. Corsetti, 1987: A fast radiation parameterization for general circulation models. *J. Geophys. Res.*, 92, 1009-1016.

Jarvis, P. G., 1976: The interpretation of the variations in leaf water potential and stomatal conductance found in canopies in the field. *Phil. Trans. Roy. Soc. London,. B.* 273, 593-610.

Kim, J.-W., 1976: A generalized bulk model of the oceanic mixed layer. *J. Phys. Ocean.*, 6, 686-695.

Mahrt, L., 1981: The early evening boundary layer transition. *Quart. J. Roy. Meteor. Soc.*, 107, 329-343.

Randall, D. A., 1979: The entraining moist boundary layer. Paper presented at the *Fourth Symposium on Turbulence, Diffusion, and Air Pollution of the Amer. Meteor. Soc.*, Reno, Nev., 476-470.

Randall, D. A., 1984: Buoyant production and consumption of turbulence kinetic energy in cloud-topped mixed layers. *J. Atmos. Sci.*, **41**, 402-413.

Raupach, M. R. and Thom, A. S., 1981: Turbulence in and above plant canopies. *Ann. Rev. Fluid Mech.*, **13**, 97-129.

Sellers, P. J., Y. Mintz, Y. C. Sud, and A. Dalcher, 1986: A simple biosphere model (SiB) for use within general circulation models. *J. Atmos. Sci.*, **43**, 505-531.

Sun, S. F., 1982: Moisture and heat transport in a soil layer forced by atmospheric conditions. M. Sc. Thesis, University of Connecticut, Connecticut, U.S.A., 72 pp.

Suarez, M. J., A. Arakawa, and D. A. Randall, 1983: Parameterization of the planetary boundary layer in the UCLA general circulation model: Formulation and results. *Mon. Wea. Rev.*, **111**, 2224-2243.

van der Honert, T. H., 1948: Water transport as a catenary process. *Discuss. Faraday Soc.*, **3**, 146-153.

Willmott, C. J. and K. Klink, 1986: *A representation of the terrestrial biosphere for use in global climate studies.* European Space Agency, Paris, France, 109-112.

Zilitinkevich, S. S., 1975: Comments on "A model for the dynamics of the inversion above a convective boundary layer." *J. Atmos. Sci.*, **32**, 991-992.